College of Engineering

Drexel E-Repository and Archive (iDEA)
http://idea.library.drexel.edu/

Drexel University Libraries
www.library.drexel.edu

Please direct questions to archives@drexel.edu

Design and microfabrication a high-aspect-ratio PDMS microbeam array for parallel nanonewton force measurement and protein printing

F Mert Sasoglu, Andrew J Bohl, and Bradley E Layton
Drexel University, Department of Mechanical Engineering and Mechanics
3141 Chestnut St, Philadelphia, PA 19104

E-mail: blay@drexel.edu

Abstract. Cell and protein mechanics has applications ranging from cellular development to tissue engineering. Techniques such as magnetic tweezers, optic tweezers, and atomic force microscopy have been used to measure cell deformation forces on the order of piconewtons to nanonewtons. In this study, an array of polymeric polydimethylsiloxane (PDMS) microbeams with diameters of 10-40µm and lengths of 118µm was fabricated from Sylgard® with curing agent concentrations ranging from 5% to 20%. Resulting spring constants were 100-300nN/µm. The elastic modulus of PDMS was determined experimentally at different curing agent concentrations and found to be 346kPa to 704kPa in a millimeter-scale array and ~1MPa in a microbeam array. Additionally, the microbeam array was used to print laminin for the purpose of cell adhesion. Linear and non-linear finite element analyses are presented and compared to the closed-from solution. Conclusion: The highly compliant, transparent, biocompatible PDMS may offer a method for more rapid throughput in cell and protein mechanics force measurement experiments with sensitivities necessary for highly compliant structures such as axons.

PACS number: 74B20, 74K10, 74E30

Keywords: microbeam array, force measurement, PDMS, cell mechanics, laminin printing

1. Introduction

The primary objective of this paper is to demonstrate a method for design and fabrication of a highly compliant microbeam array for measuring cell stiffnesses in a highly parallel manner. The high-aspect-ratio, compliant beams may also be used to print arrays of proteins such as laminin on various surfaces for applications such as cell printing.

Living cells change shape in response to applied mechanical forces e.g. (Vandenburgh and Kaufman 1979). In neurons, extended processes known neurites, which have the potential to develop into axons have been shown to be initiated *in vitro* by localized application of tensile forces (Bray 1984; Dennerll *et al.* 1989). While this has been achieved previously with glass (Zheng *et al.* 1991; Chada *et al.* 1997), we have chosen the soft material polydimethylsilixone (PDMS) for our microbeams for its mechanical compliance, optical transparency, manufacturability and biocompatibility (Zhao *et al.* 2005). Other attractive attributes of PDMS are its usability over a wide temperature range (-100°C to 100°C), low chemical reactivity, and non-toxicity (Lotters *et al.* 1997). PDMS has a relatively small modulus of elasticity, 100kPa – 1MPa, e.g. (Carrillo *et al.* 2006) making it favorable for measuring stiffnesses of cell structures such as axons, which are know to be highly mechanically compliant ~10pN/µm (Kis *et al.* 2002), red blood cells ~20pN/µm (Liu *et al.* 2006) or chondrocytes which have been shown to have stiffnesses of approximately 20nN/µm (Shieh and Athanasiou 2006). To achieve the goal of measuring deflection optically, where resolution is limited to ~0.5μm, the stiffness value of the microbeams should be of the same order of magnitude as the specimen. By measuring the deflection and knowing the stiffness values of the beams both analytically and experimentally, the mechanical properties of cellular substructures such as axons or neurites may be determined. A schematic of the proposed strategy is shown in Figure 1.

A variety of reasons exist for performing such force-deflection measurements. Examples include understanding the effects that various cytoskeletal proteins have in determining the mechanical properties of axons (Ingber 2003), understanding the role that various pharmaceuticals play in affecting neural growth characteristics (Bell 1996), and understanding the effects that various neurotoxins have on neural growth characteristics (Li *et al.* 1998).
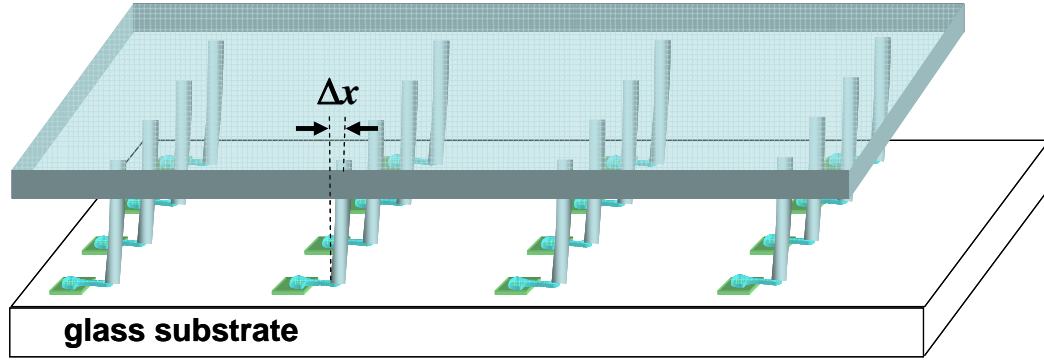
Figure 1. A schematic of the proposed parallel force measurement strategy. Printed cells are interrogated from above with an array of microbeams. Relative displacement, Δ*x*, is measured between the stationary cells and the actuated microbeam array. The green square patches represent printed laminin and the structures tethered between the laminin patches and the tips of the microbeams represent the cells under mechanical tension.

Other potential technologies for measuring cell stiffness include MEMS-based microgrippers e.g. (Layton *et al.* 2005), which have been previously designed to manipulate microscopic objects (Lee *et al.* 2003). Atomic force microscope (AFM) tips, with relatively large stiffnesses values (μN/μm), when used in conjunction with a photodiode array can measure forces on the order of pN e.g. (Jacot *et al.* 2006) and have been used in torsion mode to measure small forces e.g. (Bhushan and Kasai 2004). However, these methods occlude the view of the cells, while the transparent PDMS array does not. Other force measurement devices include piezoelectrics (Rogers *et al.* 2004), but have yet to gain widespread use for single cells. Laser tweezers also offer an attractive method for nanoscale force measurement (Liu *et al.* 2006), but these have yet to be used in parallel (Danilowicz *et al.* 2005). Magnetic bead force application is another attractive and increasingly popular mode for its high sensitivity e.g. (Fass and Odde 2003), and has recently been used in parallel systems (Danilowicz *et al.* 2005), but has not yet been demonstrated in a regular array pattern for cellular force measurement applications. Among other candidate technologies for nanoscale force measurement are carbon fiber beams (Nishimura *et al.* 2004) or carbon nanotubes (Salvetat *et al.* 1999), however difficulties in spatial ordering, and potential cytotoxicity e.g. (Sayes *et al.* 2006), make this approach less attractive for cell mechanics experiments. Herein, we parameterize the geometry of a PDMS microcone array and present a microfabrication and actuation strategy to impose forces on cellular components such as axons in order to understand the roles of particular cytoskeletal and molecular-motor-driven forces in the growth, maintenance and regeneration of nerves. A comparison of the various approaches and our proposed method is given in Figure 2.

3
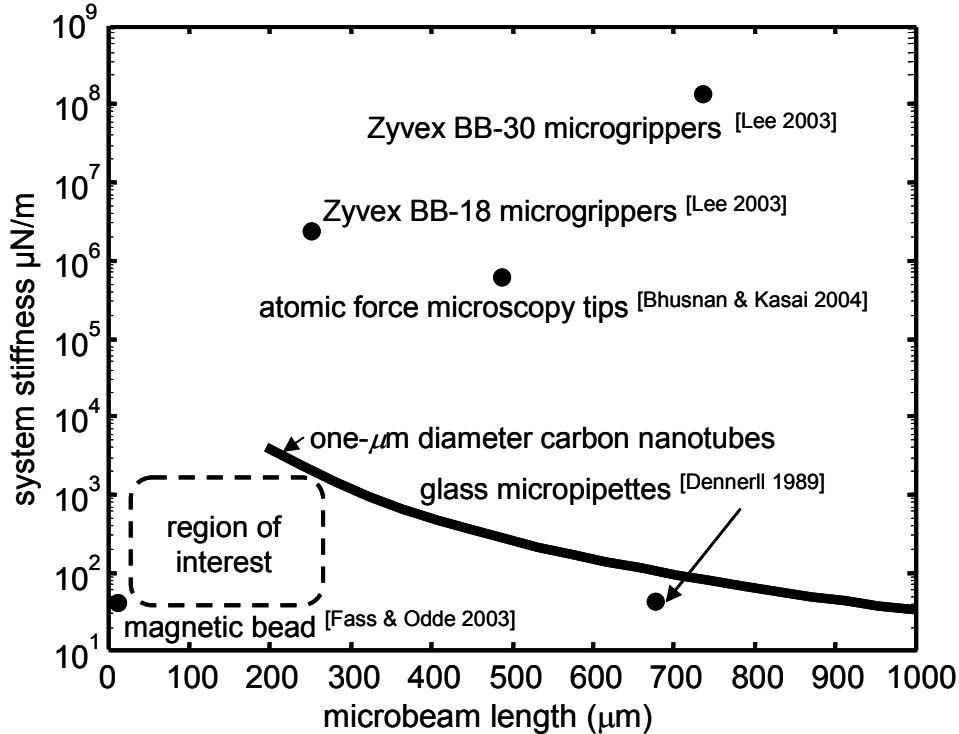
Figure 2 . Comparison of previous approaches and potential approaches to measure cell stiffness. Our proposed design is one million times more compliant than silicon microgrippers of similar dimension, two orders of magnitude more compliant than carbon nanotubes of same size, and five orders of magnitude more compliant than AFM tips. The length given for the magnetic particle is that of the particle diameter used by Fass and Odde. For a comprehensive review of additional microscale and nanoscale force measurement techniques see Van Vliet *et al.* (2003).

For parallel force measurement in cells, an adhesive substrate must be provided. A popular material substrate for adhering neurons has been laminin e.g. (Yang *et al.* 2005). Laminin is a large, basement membrane glycoprotein with diverse biological functions including differentiation, migration, and adhesion of cells. Its cell binding ability (via membrane-bound integrin receptors) makes laminin an effective substrate coating for stimulating and enhancing cell migration and neurite outgrowth. Laminin-5 is a basement membrane extracellular matrix macromolecule that provides an attachment substrate for both adhesion and migration in a wide variety of cell types, including epithelial cells, fibroblasts, neurons and leukocytes (Koshikawa *et al.* 2000). The most common methods for laminin patterning are microcontact printing (De Silva *et al.* 2004; Sgarbi *et al.* 2005) and soft lithography (Kane *et al.* 1999). Other recent research into methods of micropatterning cells on chips e.g. (Bouaidat *et al.* 2004), includes micro-contact printing (μCP) (Lauer *et al.* 2001) and hydrophobic-Teflon-patterned neural guides (Tixier *et al.* 2000; Griscom *et al.* 2002; Griscom *et al.* 2002).

4

Network arrays of neurons seeded on microposts have been constructed for the purpose of mechanically stimulating multiple neurons simultaneously (Baldi *et al.* 2003), however since the microbeams were made of silicon, they had a stiffness roughly six orders of magnitude greater than that of the neurons and were thus incapable of sensitive force measurement. Odde has developed a magnetic-bead approach for teasing out individual axons with a force precision of ~2-4 pN using a magnetic field with a spring constant of ~12 pN/µm (Faas and Odde, 2003). This approach is attractive for its high degree of precision, but has the drawback that only one axon may be teased at a time in a controlled manner. Other groups have recently used low aspect ratio (< 1:5) PDMS microbeam arrays cast from silicon-etched microbeams known as mPADs (microfabricated post array detectors) to measure forces on the order of a few tens to hundreds of nanonewtons per micrometer in fibroblast populations (Lemmon *et al.* 2005). This method allows the cultured cells to sit atop the microbeam array, with individual cells spanning several beamtips, actively straining the beams. By contrast, our method proposes to actively strain the cells from above with a one beamtip-to-one-cell strategy.

In the present work, we demonstrate our ability to manufacture high-aspect-ratio PDMS silicone (polymeric) microbeams with dimensions on the order of millimeters capable of measuring tens of micronewtons, and a microfabricated array with a stiffness of hundreds of nanonewtons per micrometer. Other high-aspect-ratio (1:15), untapered PDMS structures exist, but are made with the relatively costly (Madou 2002) LIGA process e.g. (Kim *et al.* 2002). High-aspect ratio PDMS structures have also been micromachined to perform small-scale cell culture e.g. (Hung *et al.* 2005). To our knowledge, the specific highly parallel one-probe-to-one-cell technique proposed herein has not been achieved or attempted for neurons patterned on a substrate e.g. (Roberts and Taylor 1983; Lamoureux *et al.* 2002). Completion of this goal will also allow us to begin to use the device for testing hypotheses related to the mechanical roles of important cytoskeletal proteins such as actin and tubulin as well as the mechanical roles of important molecular motor proteins such as myosin, dynein and kinesin e.g. (Baas 1998; Yu *et al.* 2001; Baas *et al.* 2006). Specifically, it is assumed that the cytoskeleton, rather than the cell membrane, accounts for the majority of the stiffness of cell processes such as axons (Janmey 1991; Maksym *et al.* 2000; Wang and Stamenovic 2000). Subsequently, if the expression rates, spatial distributions, or interconnectivity of these cytoskeletal elements via motor proteins is altered, changes in mechanical properties will presumably result (Canadas *et al.* 2002). Furthermore, successful implementation of our highly parallel force measurement system may also have implications for regrowth strategies for the central nervous system (Gold *et al.* 2005; Hata *et al.* 2006).

2. Theory and computations

To determine the stiffness of cells by direct optical measurement, where a beam tip is brought into contact with a cell surface, the force on the beam tip is equal and opposite to the force on the cell

$$F_{cell} = F_{beam},$$ (1)

where F_{beam} is the force on the microbeam and F_{cell} is the force on the cell. Written in terms of deflection, x, and the stiffness, k,

$$\int_0^{x-x_{beam}} k_{cell}(x)dx = \int_0^{x_{beam}} k_{beam}(x)dx.$$ (2)

In the case of an Euler beam with isotropic mechanical properties loaded with one end fixed and the other end free, linear beam theory is accurate to 5% up to a beam tip deflection of 30% of the beam length. Above this deflection, nonlinear theory must be used (Belendez *et al.* 2002). In our experiments the beam aspect ratios were between 3.0 for our microbeam array and 7.5 for our millimeter scale beam array. Using a Timoshenko beam model improves the accuracy by a factor of 6% and 1% respectively (Gere and Timoshenko 1997).

2.1 Small deflection theory

The stiffness value of a single microbeam is derived using the general form of the Euler equations (Gere 2004),

$$\frac{d^2}{dx^2}\left[EI(x)\frac{d^2v(x)}{dx^2}\right] = F(x).$$ (3)

which is generally considered accurate to 10% for beam structures with aspect ratios of ten or greater. A cylindrical beam with constant modulus of elasticity, i.e. no gradient in material properties, and constant moment of inertia, has a stiffness of

$$k_{circularbeam} = \frac{3E\pi r_B^4}{4L^3}.$$ (4)

For a conical beam with a base greater than its tip, and a constant taper, the stiffness value of a single conical microbeam is derived from the same formula and expressed as

$$k_{cone} = \frac{3E\pi r_B^4 a}{4L^3},$$ (5)

6

where E is the elastic modulus, r_B is the base radius, L is the beam length and $(0 \leq a \leq 1)$ is the tip-diameter to base-diameter ratio. Equation (5) shows that by keeping the base diameter constant and having the beams tapered, more compliant beams are obtained. Plots of (5), in the region of interest are depicted in Figure 3.
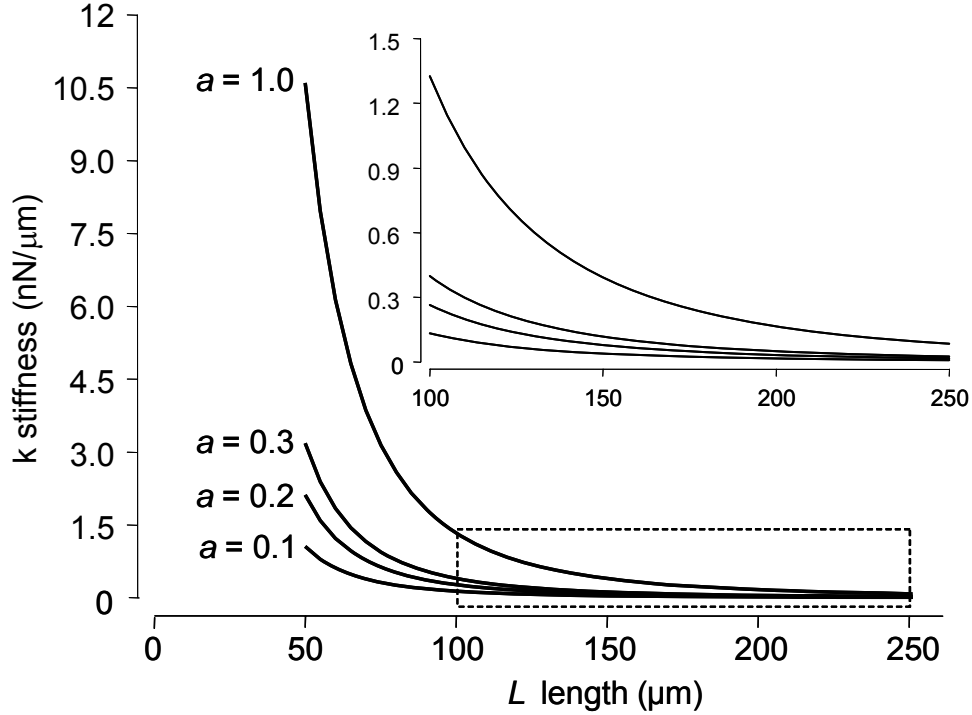
Figure 3. Beam stiffness, k, as a function of beam length, L, with a beam diameter of 10μm and taper ratios, a, ranging from 0.1 to 1.0. Inset depicts the highlighted region. The curves represent a relationship of $1/L^3$. The modulus, E, used here was 900kPa, a value within the range of our experimental results shown below.

2.2 Large deflection theory

Large deflection was simulated using the commercially available software ANSYS. For small deflection theory, the analytical solution and ANSYS give similar results, but are only valid when small deflections are applied. Large deflection theory is valid for both large and small deflections. Large static deflection theory assumes a non-linear model and therefore it is valid for the non-dimensional loading parameter, $\alpha = FL^2/2EI$ of less than 0.25 in Euler beams (Belendez *et al.* 2002). Contrary to small deflection theory, a linear approach, which is valid for small tip forces, minimal beam curvature, and loading perpendicular to the beam axis, large deflection theory produces accurate predictions under larger load, greater beam curvature, and a load that does not remain perpendicular to the beam axis.

2.3 Finite element analysis of microbeams

To evaluate the deviation from the exact solution inherent in the general form of the Euler equations, beam stiffness was also modeled using finite element analysis. Finite element analysis was preformed with ANSYS using 3D solid tetrahedral 10-node elements. The PDMS microbeams were considered isotropic with an elastic modulus of 1.1MPa and Poisson's ratio of 0.45. We used this modulus as it was what we found from characterization of the microbeams, (*3.1.2*). Although some anisotropy may have been induced by our microfabrication methods (see discussion section), we used only one loading mode to characterize our beams, and thus used isotropy as an approximation.

Two approaches were used in the ANSYS simulations: small static deflection theory and large deflection theory. For both of these approaches, two different boundary conditions were used: one with the beam tip free in two directions, and the other with the beam tip constrained along the beam axis (Figure 4). The former boundary condition more accurately represents our proposed experimental conditions, where cellular processes such as neurites are to be attached to the tips of the beams. The second boundary condition was used to simulate axial forces that may be present in the beams due to tensile forces caused by adhesion to the sample or substrate. Since large deflection theory allows for the tip force to deviate from being perpendicular to the beam axis.
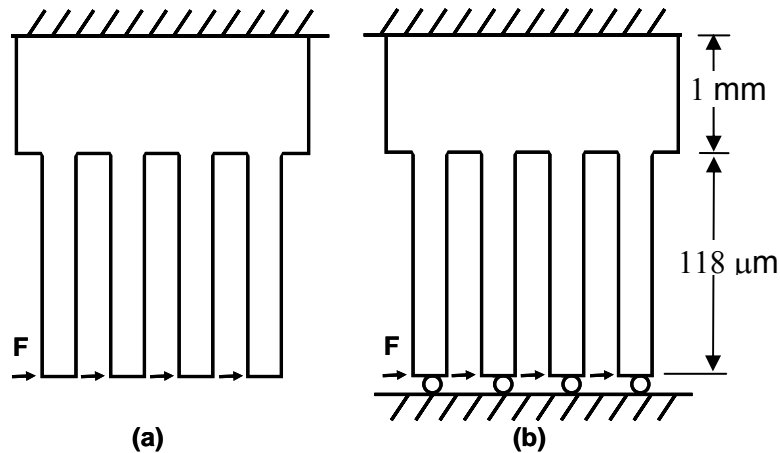
Figure 4. Boundary conditions for FEA. In both cases, displacement was fixed at the beam bases (top of the figure) (a) free tips. (b) tips with the axial degree of freedom fixed. The drawing is to depict boundary conditions and is not to scale. The out-of-plane dimension was 1mm.

3. Fabrication and mechanical testing

3.1 Fabrication of large-scale prototype for obtaining PDMS properties

3.1.1 Fabrication. A steel master template was fabricated from a 3.75-mm-thick stainless-steel master mold using conventional drilling methods on a Haas TM2 CNC mill. A square array of sixteen holes was drilled, each through-hole having a diameter of 500μm and a depth of 3.75mm. PDMS prepolymer (Sylgard 182, Dow Corning), with an average pre-cured polymer chain length of 300 mers (~90nm long with a bonding radius of 1.5 Å between the Si – O backbone) was prepared by mixing the resin with curing agent at four ratios (5%, 7%, 10% and 20% by weight) in a mixer attached to a hydraulic dispenser (Mixpac System 200). It was then kept ready in a Petri-dish at room temperature to pour into the injection vessel (Figure 5a). The steel mold was placed inside the injection vessel; PDMS was poured in, the cap screwed onto the end of the vessel and a vacuum applied to pull the PDMS through the mold. Just after pouring the PDMS prepolymer into the injection vessel, it was degassed under vacuum at 25 inches of Hg (85 kPa) for approximately 30 minutes to eliminate bubbles. After inserting the steel mold into the vessel, a pressure difference of 40 kPa was applied to the vacuum tube to induce PDMS flow into the mold. The required pressure difference, Δp, for a through-hole may be calculated using the Young-Laplace equation (Pellicer *et al.* 2000),

$$\Delta p = \frac{2\sigma \cos\theta}{r}, \tag{6}$$

where σ is the surface tension, θ is the contact angle measured in liquid and r is the radius of the fluid surface. If θ is greater than 90º, the liquid is non-wetting with the solid surface, rendering Δp negative and thus fluid must be pumped into the hole. However, if θ is less than 90º Δp is positive and no pressure must be supplied to drive the wetting fluid into the opening. The contact angle must be determined experimentally. We have observed experimentally that the contact angle is greater than 90º implying that pressure should not be required to drive the fluid into the hole. However, in this case, capillary flow into the holes was not observed at least over the timescale of minutes, presumably due to high viscosity of the uncured polymer. Afterwards, the mold was put into an oven for curing at 80° C for 120 minutes. It was then peeled from the mold after freezing at -70º C for 1 hour. This is necessary due to the surface interactions between the PDMS and the rough steel surface: PDMS has a coefficient of thermal expansion thirty times less than that of steel, and thus pulls away from the inner steel surface during freezing.

3.1.2 Mechanical characterization. The beam array was placed horizontally and lowered onto an Accu-224 precision analytical balance (Fisher Scientific) with a sensitivity of 0.1mg

(1μN) so that only the tip of the beams touched the balance (Figure 5b). Balance deflection was measured to be negligible (12μm deflection under a 300mN load, or <0.1% of our calibration loads), so tip deflection was taken to be that of the micrometer reading. The micrometer used was a M3301 three-axis micropositioner with a precision of 10μm (World Precision Instruments, Sarasota, Florida). Tip force was read directly from the balance. We took force readings at deflections of 100μm, 200μm, 300μm, 400μm, and 500μm and fitted the results to $F = kx$, using linear regression finding k for each beam. This process was repeated three times on each of three different beams within the sixteen-beam arrays at each curing agent percentage. The elastic modulus was determined by using the analytically derived deflection formula for circular cross-sectional beams (4) for the four curing-agent to base-agent ratios.
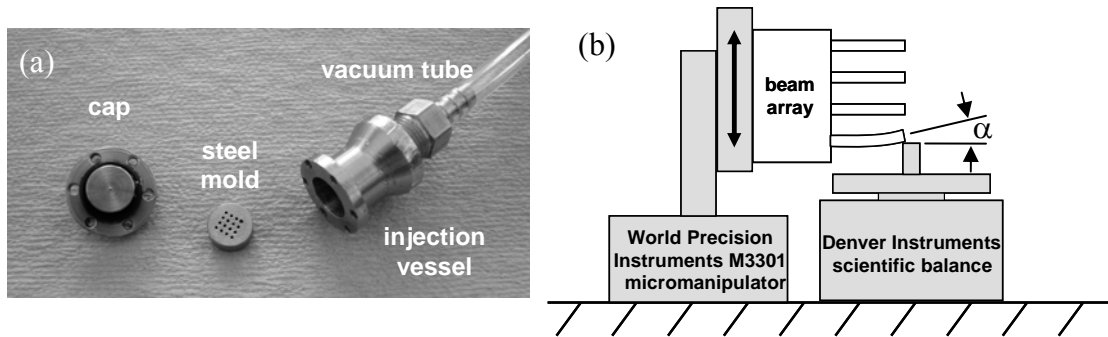

Figure 5. (a) The injection vessel designed for fabricating the large beam array with through-holes. (b) The micromanipulator and balance configuration used to measure beam stiffness for the larger beams. Force was recorded from the balance and deflection recorded from the manipulator. The angle α depicts that of the beamtip axis with the beam base axis.

3.2 Microfabrication and characterization of the microbeam array

3.2.1 Microfabrication. Photolithography was used to fabricate a 100 x 100 microbeam array mold in preparation for PDMS replica molding. A darkfield chrome photomask fabricated by J.D. Photo Tools (Oldham, Lancs, UK) was printed onto soda lime glass with a thickness of 1.5 mm. A layer of negative photoresist, SU-8 2035 was spin-coated onto 3.175-mm-thick borosilicate at 500 rpm, 100 rpm/s for 10 seconds and 750 rpm, 300 rpm/s for 30 seconds with a Brewer Science CEE100 spin coater, resulting in a thickness of approximately 200 μm. It was then soft baked at 65° C for 5 minutes and ramped to 95° C for 20 minutes and slowly cooled to room temperature. The assembly was then exposed to UV light (365 nm) for 15 seconds under the mask at an intensity of 25mJ/sec·cm^2. Post baking was performed to selectively cross-link the portions exposed to UV-light. The SU-8 was developed with PGMEA solution to obtain the

desired micromold. The PDMS mixture was prepared at a ratio of 10:1 and poured onto the SU-8 mold. It was then degassed for approximately two hours to eliminate bubbles and cured at 80°C for approximately two hours. It was then peeled from the mold to obtain the desired geometry (Figure 6).

For the non-through holes, as used in our microfabrication process, air from the bottom of the holes must be removed if the microbeams are to become fully formed. This requires movement of a 1-10 μm diameter air bubble from the bottom of a hole, typically with a vacuum source. As the dimensions of the device are reduced this becomes increasingly difficult as evidenced by the pitting present on the PDMS microbeams presented by Schmitz *et al.* (2005).
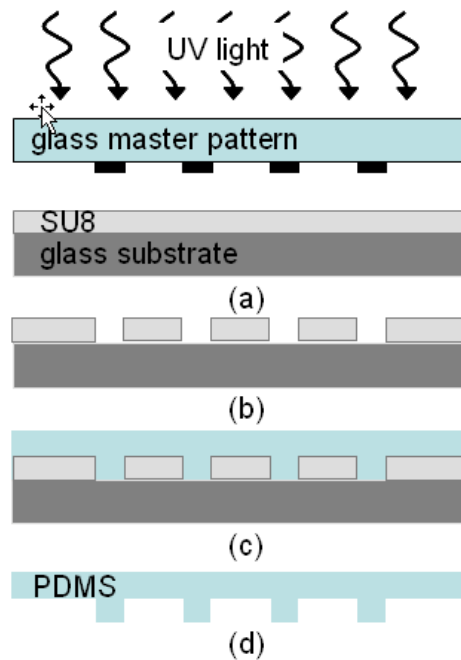
Figure 6. Schematic of the microfabrication process. (a) UV light is exposed to a thin layer of SU8 that has been deposited on a silicon substrate to produce the pattern. The light is passed through a glass pattern that has an opaque black plastic printed on it. (b) The unexposed portions are etched away to reveal a three-dimensional negative of the array. (c) PDMS is poured over the pattern and subjected to vacuum such that it fills all available space and air is allowed to escape. (d) The PDMS is peeled away from the mold, resulting in the final microbeam array.

3.1.2 Mechanical characterization of the microbeam array. Calibration of twenty-five beams from one of the 40-μm-diameter, 100-μm-long PDMS microbeam arrays was calibrated under light microscopy with a 20x objective (200x total magnification) with an Olympus IX81 inverted microscope (Figure 7). The microbeam array was mounted on the edge of a standard 1" x 3" glass slide with the beams oriented horizontally. A pre-calibrated cantilever with a stiffness

of 215 nN/µm (Veeco Probes, Santa Barbara, CA) was mounted at the end of an Eppendorf NK-2 micromanipulator and brought into contact with a single beam within the microbeam array. The micromanipulator was then moved a total of 40 µm in steps of approximately 5µm. Deflection of both the cantilever tip and microbeam tip were measured from images captured with a SPOT-RT camera according to $k_{beam} = k_{cantilever}(40µm-\delta_{cantilever})/\delta_{microbeam}$.
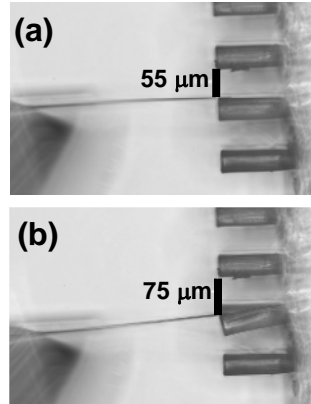

Figure 7. Mechanical characterization of one PDMS microbeams (right) with a precalibrated silicon Veeco Probes cantilever (left). (a) Initial contact is made. (b) At a PDMS beam tip displacement of 20µm shown here, the silicon cantilever displacement is approximately 15µm.

4. Laminin printing

The high-aspect-ratio microbeam array was used to print laminin on a cover slip to be used as a pattern for cell attachment. Natural mouse laminin 23017-015 (Invitrogen) was mixed with 0.05 M TRIS base with a pH of 10.9, and 0.15 M NaCl in a Petri-dish at a concentration of 20 µg/ml. The mixture was deposited onto the patterned side of the microbeam array for 30 minutes and dried with a nitrogen stream (Sgarbi *et al.* 2004). A mass of 10 g was put onto the microbeam array for five minutes to achieve full contact between the array and the cover slip. The printed array was washed once with deionized water to wash away unattached laminin.

5. Results

5.1 Fabrication results

After release, the large-scale beam array was sputtered with a 10 nm coating of platinum and imaged at 10 kV in an Amray 1860 scanning electron microscope (Figure 8a). Immediately observable are the fractured surfaces of the beam tips. This was due to the cleaving of the tips prior to release and after freezing.

By varying SU-8 film thickness, UV exposure energy, developing time, and agitation rate during developing, we were able to manufacture tapered microbeams (Figure 8b) in addition to the non-tapered microbeams depicted in Figure 7. If the mask and substrate assembly is placed at an angle to the UV source, tapered holes are achieved. Another way to obtain conical sidewalls is over exposure of the top portion of the resist film, resulting in tapered sidewall profiles. However, it is difficult to control the angle by changing the exposure time. The beam length consistency was measured with a Zygo optical profilometer (Model #NV6200) and found to be 118.4 ± 0.2 µm. The tapered beams are theoretically less stiff than corresponding straight-walled beams (5). Tapered beams also enable smaller laminin base locations for cell attachment during the micro-printing process.
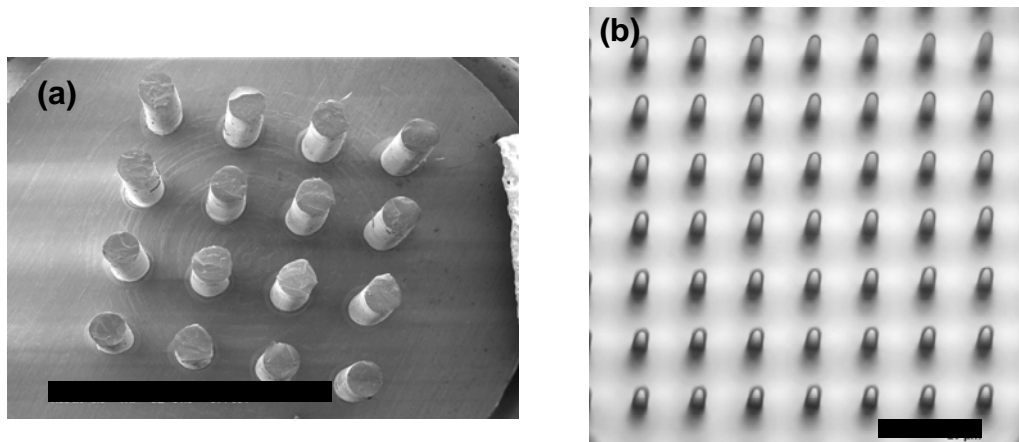

Figure 8 a) SEM image of a fabricated macroscale prototype of 4x4 array. Scalebar = 4mm b) Optical micrograph of a portion of the microfabricated tapered PDMS 100 x 100 microbeam arrays. The base diameters of the beams are approximately 10 μm and the length is approximately 100 μm. Scalebar = 100µm.

5.2 PDMS properties vs. curing agent volume fraction

Stiffness curves for the millimeter-scale beam array was measured by simultaneous recording of the micropositioner travel and the force on the scientific balance with the PDMS cantilever beam tip under load (Figure 9). Since the balance can only record the force perpendicular to the beam axis, and the final angle under full load was approximately 30 degrees, a factor of 1/cosα (Figure 5) was used to scale the modulus values resulting from the stiffness curves. The beam stiffnesses were found to increase with increasing volume fraction of curing agent. Curing agent percentage affected stiffness significantly up to 10%. Adding more curing agent shows only a slight increase in the stiffness. Adding curing agent less than 7% prevents full

PDMS solidification. Therefore, the optimum value to obtain the lowest stiffness, while maintaining a solid beam is between 7-10%.
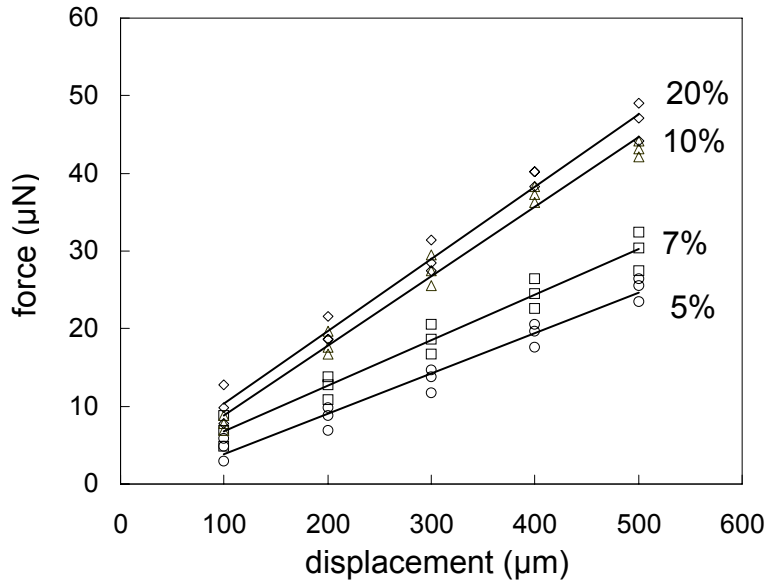
Figure 9. Force-displacement curves from the large PDMS array used to determine beam stiffness, *k*, as a function of curing agent percentage. Each symbol represents the average force from a single beam. *n* = 9 for each linear regression line.

5.3 Calibration of microbeams

Shown in Figure 10 are the results of calibrating a microbeam array with beam diameters of 40μm compared to those with a 500μm diameter. The elastic modulus of PDMS for the four different curing agent concentrations (5%, 7.5%, 10%, and 20% by weight) resulted in moduli of 346 ± 22, 473 ± 37, 589 ± 23, and 704 ± 29 kPa (Figure 10). An increase in elastic modulus at small scales has been seen previously for hydrogels e.g. using AFM indentation (Harmon *et al.* 2003) and in silicon (Sundararajan *et al.* 2002). In the Harmon paper, AFM was performed on spin-coated thin films, and loaded in out-of-plane direction. The Sundarajan work used a three-point bending method and attributed their variations to inconsistencies in crystal lattice orientation, and perhaps fewer defects in their single-crystal preparations. Anisotropy has also been found in other spin-coated PDMS preparations where the polymer chains align with the flow direction (Elzein *et al.* 2004). Others who performed AFM indentation on the surface of polymeric materials concluded that the small-scale material properties are consistent with the bulk properties to a scale of 40nm (Tranchida *et al.* 2006). However, the materials used by Tranchida *et al.* were not prepared with the extrusion/injection method of the current work, and thus are likely to be more amorphous.
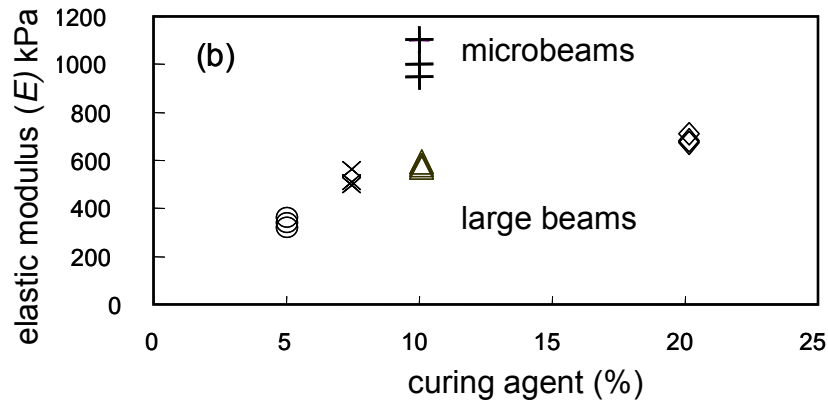
Figure 10. A comparison of the elastic moduli measured from the millimeter scale array compared to that measured in the micrometer scale array.

5.4 FEA results

Microbeams were modeled as either fixed at the base and free at the tip, or fixed at the base and fixed against axial displacement at the tip. Loads up to 5000 nN in increments of 1000 nN were applied for each case using linear theory and non-linear theory. The closed-form solution was obtained using the stiffness formulation of the Euler-beam equation (4) and the known tip force. For deflections smaller than 3 μm, linear and nonlinear results give results with approximately 1% error. For the fixed-fixed boundary conditions, a closed-form solution may not be obtained by linear methods and thus only the numerical results are shown. Since the experimental loading conditions were such that the force on the tip of the PDMS microbeam did not remain perpendicular to its axis, a cosine factor commensurate with the angle observed was used to find the angle adjusted result (Figure 11). Additionally, the reason that the experimental results are concave down is perhaps due to the fact that as the PDMS beam deflects, approaching its own substrate, the bending force of the silicon cantilever required to maintain this bending force actually decreases. In this limit, the force on the calibration cantilever becomes a purely axial force, which would hold the PDMS microbeam pinned against its own substrate. In this scenario, the bending of the silicon cantilever could potentially be zero whereas the bending angle of the PDMS microbeam would be 90°, yielding a result of infinite compliance, or zero stiffness. Thus the downward concavity seen in the experimental curve of Figure 11 could continue until it ultimately hit the abscissa.
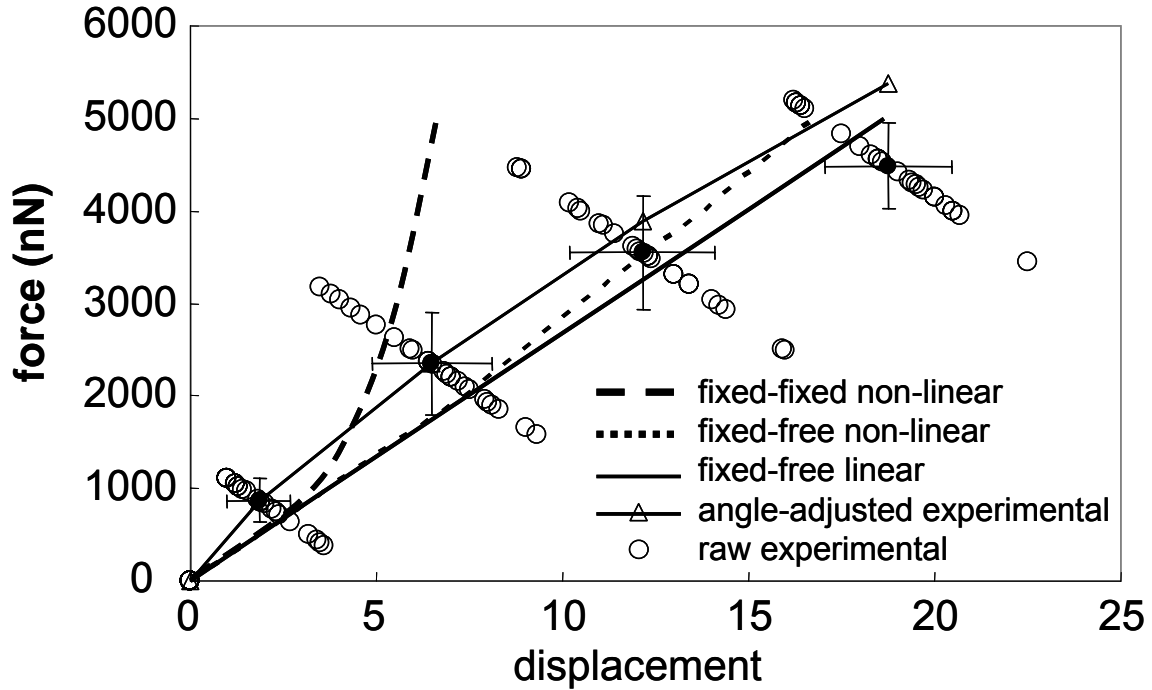
Figure 11. FEA results using the beam geometry of the microbeam device shown in Figure 8b. The linear solution is a straight line and coincides with the closed-form solutions. The non-linear solution shows the effect that a finite angle at the beam tip produces. In the fixed-fixed solution, the additional apparent stiffness is a result of the axial tensile force at the beam tip being amplified in the transverse direction.

5.5 Laminin printing results

While our primary intended utility of the microbeam array is to achieve parallel force measurement on structures such as cells at the microscale and ultimately the nanoscale, it may also be used to print proteins. Having a laminin grid spacing that equals the beam tip spacing will facilitate alignment for planned neuron straining experiments. The microbeam array was used to print laminin on a glass cover slip in a pattern identical to the intended cell array pattern. After a mass of 10 g was put onto the array for five minutes to obtain the full contact between the microbeam array and the cover slip to obtain uniform printing, the microbeam array was removed, revealing the intended pattern (Figure 12).
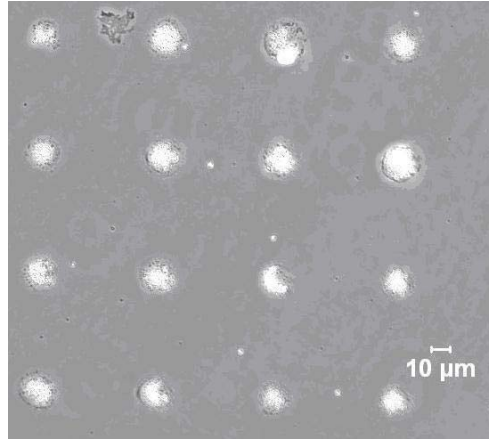
Figure 12. Brightfield optical microscopy image of mouse laminin printed on a glass coverslip revealing a pattern identical to the microbeam array and the intended cell printing pattern. A laminin substrate is critical to cell adhesion. The non-printed regions will allow for unhindered force measurement, since cells will experience less surface interaction force within this region.

6 Discussion and future work

The low modulus of elasticity, biocompatibility, and transparency of PDMS make it an ideal candidate for force transduction in highly compliant cells such as axons. We have tuned the modulus of elasticity of PDMS with curing agent and found an optimum value for having a solid PDMS beam with the smallest modulus of elasticity is between 7% and 10%. To examine the effect of miniaturization, mechanical testing was performed to obtain the elastic modulus of smaller beams. The elastic modulus of the small beams was found to be greater (~1.1 MPa) than that of the large beams (~600 kPa). The resulting stiffnesses are still on the order of 200nN/μm, or four orders larger than our target value. However, since stiffness, k, scales by the fourth power of beam thickness, once we achieve 4 μm diameter beam dimensions (ten times smaller), our stiffness will diminish by a factor of ten-thousand, putting us in the exact range we are targeting. This we expect to be achievable with more precise photolithography masks. As stated previously, our goal is to achieve beams with stiffnesses on the order of 10pN/mm, or approximately that of the neurons under investigation.

We have achieved an aspect ratio of ten with by photolithography followed by PDMS replica molding. We found that photolithography developing time greatly affected hole depth and sidewall straightness. Over exposure and less developing times result in arrayed beams with tapered sidewalls. As aspect ratios grow and overall diameters shrink, we expect to find an

17

enhanced trend in the scale-dependence of stiffness. This stiffening scale effect has been seen previously in silver nanowires (Jing *et al.* 2006) and was attributed to surface effects. Since the Si – O backbone of our system is clearly different from the presumably crystalline structure of the Ag nanowires of the Jing paper, the physics are clearly different. However, since we clearly saw stiffness decreases in the millimeter-scale beams as curing agent percentage diminished, we can conclude that the degree of crosslinking affects stiffness. One other possible explanation for the subtly increased stiffness is that the holes into which the microbeams were cast, preferentially excludes polymer chains and enhances crosslinking agent concentration, thus enhancing stiffness. This could have the effect of lengthening the post-curing polymer chains.

Individual polymers tend to align with the primary flow direction during fabrication e.g. (Huang *et al.* 2001; McFarland and Colton 2004). Polymer chain alignment is shear rate dependent (Cormier and Callaghan 2002), and can induce crystallization (Somania *et al.* 2005). Polymer chain orientation in surface-treated PDMS has been induced previously by mechanical stretching experiments and shown to affect hydrophobicity (Genzer and Efimenko 2000). Polymer chain orientation has also been induced mechanically in PDMS to modify optical properties (Tanigaki *et al.* 1998). Longer chained PDMS molecules have also been shown to show diminished surface friction properties (Galliano *et al.* 2003), thus these would not necessarily be impeded from entering the microfabricated holes in our system. It may be useful in future studies to incorporate X-ray diffraction studies to quantify polymer chain alignment and to examine how the theoretical radius of gyration (Lapp *et al.* 1985) in a bulk melt differs from that of a micromanufactured system. We expect that as we attempt to create higher aspect ratio structures that this anisotropy will be enhanced.

Another important consideration for using these structures in fluid is that in the non fully crosslinked state, they may tend to absorb water, thus altering the mechanical properties and perhaps causing unwanted deformation due to inhomogeneities. An experiment using a force measurement device such as ours would require either constant or periodic calibration if it were to be used for hours or days. While calibration of individual microbeams against a known standard would not be practical during a cell mechanics experiment, running a calibration on a few beams against a standard during an experiment would be necessary to track hydration effects.

A Matlab code is being developed to obtain the displacement of the beams while stretching cells. Having the deformed and undeformed bottom view of the beams under the microscope, the code calculates the displacement of the center of the beams from the images. The beams are positioned such that the tips of the beams simultaneously touch the glass slide and are visible from below with an inverted microscope. The initial configuration and the instantaneous

positions of the microbeams at different timelines during stretching process are then captured using camera software. The images are then converted within Matlab to binary images to obtain the circular outer borders of the beams. From this displacement of each beam is calculated by subtracting the center of the individual circular spots at the initial configuration and the displaced configurations. The code then determines the force applied to the cells using (1) and (2) to obtain the stiffness of each cell.

There are two primary long-term objectives of this project. One is to use the device to test hypotheses regarding the contributions of specific protein structures such as actin and tubulin and specific molecular motors such as myosin and kinesin on axonal growth mechanics e.g. (Baas *et al.* 2006). The nerve cells will be printed such that each nerve cell body sticks to only one laminin spot which is printed using the microfabricated beam array. The microbeam array will be aligned above the cell array and allowed to adhere to the cells in a one-to-one fashion using integrin coated tips (Fass and Odde 2003). Once adherence has occurred, the cells will be stretched unidirectionally in order to measure axon stiffness and grow the axons in a controlled manner. By altering expression rates or polymerization rates of important cytoskeletal proteins such as actin or tubulin, or their associated molecular motors such as myosin, kinesin and dynein, we may be able to gain valuable quantitative insight into how the forces generated by these molecules affect axonal growth rates. The other long-term goal is to use the device to guide neurons to grow in specific patterns on an electrically active substrate in order to build neuronal-based bio-sensor devices. Compared to previous neuron-based sensors e.g. (Pancrazio *et al.* 1999; Kovacs 2003), this may have the advantage in that cell-cell interaction may be directly controlled mechanistically rather than relying on axons to follow printed guides.

References

Baas P W 1998 The role of motor proteins in establishing the microtubule arrays of axons and dendrites *J Chem Neuroanat* **14** 175-80

Baas P W, Nadar C V and Myers K A 2006 Axonal Transport of Microtubules: the Long and Short of It *Traffic* **7** 1-9

Baldi A, Fass J N, De Silva M N, Odde D J and Ziaie B 2003 A micro-tool for mechanical manipulation of in vitro cell arrays *Biomedical Microdevices* **5** 291-295

Belendez T, Neipp C and Belendez A 2002 Large and small deflections of a cantilever beam *European Journal of Physics* **23** 371-379

Bell C 1996 <u>Chemical Factors in Neural Growth Repair and Degeneration</u> Elsevier.

Bhushan B and Kasai T 2004 A surface topography-independent friction measurement technique using torsional resonance mode in an AFM *Nanotechnology* **15** 923-935

Bouaidat S, Berendsen C, Thomsen P, Petersen S G, Wolff A and Jonsmann J 2004 Micro patterning of cell and protein non-adhesive plasma polymerized coatings for biochip applications *Lab on a Chip* **4** 632-637

Bray D 1984 Axonal growth in response to experimentally applied mechanical tension *Dev Biol* **102** 379-89

Canadas P, Laurent V M, Oddou C, Isabey D and Wendling S 2002 A cellular tensegrity model to analyse the structural viscoelasticity of the cytoskeleton *J Theor Biol* **218** 155-73

Carrillo F, Gupta S, Balooch M, Marshall S J, Marshall G W, Pruitt L and Puttlitz C M 2006 Nanoindentation of polydimethylsiloxane elastomers: Effect of crosslinking, work of adhesion, and fluid environment on elastic modulus *Journal of Materials Research* **21** 535-537

Chada S, Lamoureux P, Buxbaum R E and Heidemann S R 1997 Cytomechanics of neurite outgrowth from chick brain neurons *J Cell Sci* **110 (Pt 10)** 1179-86

Cormier R and Callaghan P 2002 Molecular weight dependence of segmental alignment in a sheared polymer melt: A deuterium nuclear magnetic resonance investigation *Journal of Chemical Physics* **116** 10020-10029

Danilowicz C, Greenfield D and Prentiss M 2005 Dissociation of ligand-receptor complexes using magnetic tweezers *Analytical Chemistry* **77** 3023-3028

De Silva M N, Desai R and Odde D J 2004 Micro-patterning of animal cells on PDMS substrates in the presence of serum without use of adhesion inhibitors *Biomed Microdevices* **6** 219-22

Dennerll T J, Lamoureux P, Buxbaum R E and Heidemann S R 1989 The cytomechanics of axonal elongation and retraction *J Cell Biol* **109** 3073-83

Elzein T, Galliano A and Bistac S 2004 Chains anisotropy in PDMS networks due to friction on cold surfaces *Journal of Polymer Science Part B-Polymer Physics* **42** 2348-2353

Fass J N and Odde D J 2003 Tensile force-dependent neurite elicitation via anti-beta1 integrin antibody-coated magnetic beads *Biophys J* **85** 623-36

Fass J N and Odde D J 2003 Tensile force-dependent neurite elicitation via anti-beta 1 integrin antibody-coated magnetic beads *Biophysical Journal* **85** 623-636

Galliano A, Bistac S and Schultz J 2003 The role of free chains in adhesion and friction of poly(dimethylsiloxane) (PDMS) networks *Journal of Adhesion* **10** 973-991

Genzer J and Efimenko K 2000 Creating long-lived superhydrophobic polymer surfaces through mechanically assembled monolayers *Science* **290** 2130-3

Gere J M 2004 <u>Mechanics of Materials</u> Thomson Brooks/Cole.

Gere J M and Timoshenko S P 1997 <u>Mechanics of Materials</u> Boston, PWS Pub Co.

Gold B G, Armistead D M and Wang M S 2005 Non-FK506-binding protein-12 neuroimmunophilin ligands increase neurite elongation and accelerate nerve regeneration *J Neurosci Res* **80** 56-65

Griscom L, Degenaar P, Denoual M and Morin F 2002 *Culturing of Neurons in Microfluidic Arrays* 2nd Annual IEEE-EMBS Spec. Topic Conf. on Microtech. in Med. and Biology, Madison, WI.

Griscom L, Degenaar P, LePioufle B, Tamiya E and Fujita H 2002 Techniques for patterning and guidance of primary culture neurons on micro-electrode arrays *Sensors and Actuators B-Chemical* **83** 15-21

Harmon M E, Kucking D and Frank C W 2003 Photo-cross-linkable PNIPAAm copolymers. 5. Mechanical properties of hydrogel layers *Langmuir* **19** 10660-10665

Hata K, Fujitani M, Yasuda Y, Doya H, Saito T, Yamagishi S, Mueller B K and Yamashita T 2006 RGMa inhibition promotes axonal growth and recovery after spinal cord injury *J Cell Biol* **173** 47-58

Huang Y, Duan X, Wei Q and Lieber C M 2001 Directed assembly of one-dimensional nanostructures into functional networks *Science* **291** 630-3

Hung P J, Lee P J, Sabounchi P, Aghdam N, Lin R and Lee L P 2005 A novel high aspect ratio microfluidic design to provide a stable and uniform microenvironment for cell growth in a high throughput mammalian cell culture array *Lab on a Chip* **5** 44-48

Ingber D E 2003 Tensegrity I. Cell structure and hierarchical systems biology *J Cell Sci* **116** 1157-73

Jacot J G, Dianis S, Schnall J and Wong J Y 2006 A simple microindentation technique for mapping the microscale compliance of soft hydrated materials and tissues *J Biomed Mater Res A* **79A** 485-494

Janmey P A 1991 Mechanical properties of cytoskeletal polymers *Curr Opin Cell Biol* **3** 4-11

Jing G Y, Duan H L, Sun X M, Zhang Z S, Xu J, Li Y D, Wang J X and Yu D P 2006 Surface effects on elastic properties of silver nanowires: Contact atomic-force microscopy *Physical Review B* **73** 235409

Kane R S, Takayama S, Ostuni E, Ingber D E and Whitesides G M 1999 Patterning proteins and cells using soft lithography *Biomaterials* **20** 2363-76

Kim K, Park S, Lee J B, Manohara H, Desta Y, Murphy M and Ahn C H 2002 Rapid replication of polymeric and metallic high aspect ratio microstructures using PDMS and LIGA technology *Microsystem Technologies* **9** 5-10

Kis A, Kasas S, Babic B, Kulik A J, Benoit W, Briggs G A, Schonenberger C, Catsicas S and Forro L 2002 Nanomechanics of microtubules *Phys Rev Lett* **89** 248101

Koshikawa N, Giannelli G, Cirulli V, Miyazaki K and Quaranta V 2000 Role of cell surface metalloprotease MT1-MMP in epithelial cell migration over laminin-5 *J Cell Biol* **148** 615-24

Kovacs G T 2003 Electronic Sensors with Living Cellular Components *Proc. of the IEEE* **91** 915-929

Lamoureux P, Ruthel G, Buxbaum R E and Heidemann S R 2002 Mechanical tension can specify axonal fate in hippocampal neurons *Journal of Cell Biology* **159** 499-508

Lapp A, Picot C and Benoit H 1985 Determination of the Flory Interaction Parameters in Miscible Polymer Blends by Measurement of the Apparent Radius of Gyration *Macromolecules* **18** 2437-2441

Lauer L, Ingebrandt S, Scholl M and Offenhausser A 2001 Aligned microcontact printing of biomolecules on microelectronic device surfaces *IEEE Trans Biomed Eng* **48** 838-42

Layton B E, Sullivan S M, Palermo J J, Buzby G J, Gupta R and III R E S 2005 Nanomanipulation and Aggregation Limits of Self-Assembling Structural Proteins *MicroElectronics Journal* **36** 644-649

Lee W H, Kang B H, Oh Y S, Stephanou H, Sanderson A C, Skidmore G and Ellis M 2003 *Micropeg Manipulation with a Compliant Microgripper* Proceedings of the 2003 IEEE International Conference on Robotics & Automation, Taipei, Taiwan.

Lemmon C A, Sniadecki N J, AlomRuiz S, John L. Tan, Romer L H and Chen C S 2005 Shear Force at the Cell-Matrix Interface: Enhanced Analysis for Microfabricated Post Array Detectors *Molecular and Cellular Biomechanics* **2** 1-16

Li Y, Jiang N, Powers C and Chopp M 1998 Neuronal damage and plasticity identified by microtubule-associated protein 2, growth-associated protein 43, and cyclin D1 immunoreactivity after focal cerebral ischemia in rats *Stroke* **29** 1972-80

Liu Y P, Li C and Lai A C K 2006 Experimental study on the deformation of erythrocytes under optically trapping and stretching *Materials Science and Engineering a-Structural Materials Properties Microstructure and Processing* **423** 128-133

Liu Y P, Li C and Lai A C K 2006 Experimental study on the deformation of erythrocytes under optically trapping and stretching *Materials Science and Engineering A* **423** 128-133

Lotters J C, Olthuis W, Veltink P H and Bergveld P 1997 The mechanical properties of the rubber elastic polymer polydimethylsiloxane for sensor applications *Journal of Micromechanics and Microengineering* **7** 145-147

Madou M J 2002 Fundamentals of microfabrication : the science of miniaturization Boca Raton, CRC Press.

Maksym G N, Fabry B, Butler J P, Navajas D, Tschumperlin D J, Laporte J D and Fredberg J J 2000 Mechanical properties of cultured human airway smooth muscle cells from 0.05 to 0.4 Hz *J Appl Physiol* **89** 1619-32

McFarland A W and Colton J S 2004 Production and Analysis of Injection Molded Micro-Optic Components *POLYMER ENGINEERING AND SCIENCE* **44** 564-579

Nishimura S, Yasuda S, Katoh M, Yamada K P, Yamashita H, Saeki Y, Sunagawa K, Nagai R, Hisada T and Sugiura S 2004 Single cell mechanics of rat cardiomyocytes under isometric, unloaded, and physiologically loaded conditions *Am J Physiol Heart Circ Physiol* **287** H196-202

Pancrazio J J, Whelan J P, Borkholder D A, Ma W and Stenger D A 1999 Development and application of cell-based biosensors *Ann Biomed Eng* **27** 697-711

Pellicer J, Garcia-Morales V and Hernandez M J 2000 On the demonstration of the Young–Laplace equation in introductory physics courses *Physics Education* **35** 126-129

Roberts A and Taylor J S 1983 A study of the growth cones of developing embryonic sensory neurites *J Embryol Exp Morphol* **75** 31-47

Rogers B, Manning L, Sulchek T and Adams J D 2004 Improving tapping mode atomic force microscopy with piezoelectric cantilevers *Ultramicroscopy* **100** 267-76

Salvetat J P, Bonard J M, Thomson N H, Kulik A J, Forro L, Benoit W and Zuppiroli L 1999 Mechanical properties of carbon nanotubes *Applied Physics A-Materials Science & Processing* **69** 255-260

Sayes C M, Liang F, Hudson J L, Mendez J, Guo W, Beach J M, Moore V C, Doyle C D, West J L, Billups W E*, et al.* 2006 Functionalization density dependence of single-walled carbon nanotubes cytotoxicity in vitro *Toxicol Lett* **161** 135-42

Schmitz G J, Brucker C and Jacobs P 2005 Manufacture of high-aspect-ratio micro-hair sensor arrays *Journal of Micromechanics and Microengineering* **15** 1904-1910

Sgarbi N, Pisignano D, Di Benedetto F, Aloisi A, Nicolardi G, Cingolani R and Rinaldi R 2005 Physisorption of extracellular matrix proteins for cell cultures *FEBS Journal* **272** 277-277

Sgarbi N, Pisignano D, Di Benedetto F, Gigli G, Cingolani R and Rinaldi R 2004 Self-assembled extracellular matrix protein networks by microcontact printing *Biomaterials* **25** 1349-1353

Shieh A C and Athanasiou K A 2006 Biomechanics of single zonal chondrocytes *J Biomech* **39** 1595-602

Somania R H, Yanga L, Zhub L and Hsiao B S 2005 Flow-induced shish-kebab precursor structures in entangled polymer melts *Polymer* **46** 8587–8623

Sundararajan S, Bhushan B, Namazu T and Isono Y 2002 Mechanical property measurements of nanoscale structures using an atomic force microscope *Ultramicroscopy* **91** 111-118

Tanigaki N, Kyotani H, Wada M, Kaito A, Yoshida Y, Han E-M, Abe K and Yase K 1998 Oriented thin films of conjugated polymers: polysilanes and polyphenylenes *Thin Solid Films* **331** 229-238

Tixier A, Griscom L, Cozic K, Nagai H, Le Pioufle B, Murakami Y, Tamiya E and Fujita H 2000 *Catching and Attaching cells using an array of microholes* Proc. IEEE-EMBS Spec. Topic Microtech. in Biology and Medicine, Lyon, France, IEEE.

Tranchida D, Piccarolo S and Soliman M 2006 Nanoscale mechanical characterization of polymers by AFM nanoindentations: Critical approach to the elastic characterization *Macromolecules* **39** 4547-4556

Van Vliet K J, Bao G and Suresh S 2003 The biomechanics toolbox: experimental approaches for living cells and biomolecules *Acta Materialia* **51** 5881-5905

Vandenburgh H and Kaufman S 1979 In vitro model for stretchinduced hypertrophy of skeletal muscle. *Science* **203** 265-268

Wang N and Stamenovic D 2000 Contribution of intermediate filaments to cell stiffness, stiffening, and growth *Am J Physiol Cell Physiol* **279** C188-94

Yang I H, Co C C and Ho C C 2005 Alteration of human neuroblastoma cell morphology and neurite extension with micropatterns *Biomaterials* **26** 6599-609

Yu W, Ling C and Baas P W 2001 Microtubule reconfiguration during axogenesis *J Neurocytol* **30** 861-75

Zhao Y, Lim C C, Sawyer D B, Ronglih L and Zhang X 2005 Cellular Force Measurements using single-spaced polymeric microstructures:isolating cells from base substrate *Journal of Micromechanics and Microengineering* **15** 1649-1656

Zheng J, Lamoureux P, Santiago V, Dennerll T, Buxbaum R E and Heidemann S R 1991 Tensile regulation of axonal elongation and initiation *J Neurosci* **11** 1117-25